Supplementary information for Synergistic action in colloidal heat engines coupled by non-conservative flows

Sudeesh Krishnamurthy,[1] Rajesh Ganapathy,[2,3] and A. K. Sood[1,2]

[1] *Department of Physics, Indian Institute of Science, Bangalore - 560012, INDIA*
[2] *International Centre for Materials Science, Jawaharlal Nehru Centre for Advanced Scientific Research, Jakkur, Bangalore - 560064, INDIA*
[3] *Sheikh Saqr Laboratory, Jawaharlal Nehru Centre for Advanced Scientific Research, Jakkur, Bangalore - 560064, INDIA*

(Dated: July 6, 2022)

MATERIALS AND METHODS

The polystyrene colloidal microspheres (mean diameter, $\sigma = 2.03\mu m$) used for realization of the heat engine in our experiment were obtained from Bangslabs, USA. The particles were trapped in 10mM NaCl solution at a distance of $25\mu m$ from the surface of a coverslip by tightly focusing a NDYVO4 IR laser beam of wavelength, $\lambda_0 = 1064nm$ with a Carl Zeiss 100X objective with numerical aperture, N.A. = 1.4 mounted on a Carl Zeiss Axiovert Microscope. While trapping in a salt solution prevented double layer interactions between the particles, the sufficiently large distance from the coverslip avoided boundary effects on the system. To create two adjacent optical traps, we split the incident laser beam into perpendicularly polarized components using a polarizing beam splitter, which were then independently steered into the back aperture of the objective. Since, the vortexes created by the non-conservative forces is sensitive to parameters such as orientation of the beams, difference between their intensities, position of the focus etc., the steering process would create two distinct optical traps, despite being operated at the same power. In our experiments, however, we maintained the ratio between the intensities at $S(L2)/S(L1) = 1.33$ and studied the most general case of the coupling. The beam waist at the focal point, which indicates the region of influence of the laser was $\approx \frac{2\lambda_0}{\pi N.A.} = 480nm$ and significantly lesser than the closest separation distance between the microspheres $\approx 3.6\mu m$ used in our experiment. To mark the end points of the isochoric process and to monitor the distance from the coverslip, a very low powered red laser (Thorlabs ML101J8 Diode laser of wavelength 632 nm controlled using a Thorlabs TCLDM9 temperature controlled laser diode module) aligned at a slanting angle was shined at a distance at least $10\mu m$ from the trapped particles. The red laser was switched on only during the isochoric processes and its reflection from the bottom coverslip of the sample cell was monitored. This provided us the necessary temporal resolution to resolve the isochoric process as well as spatial resolution of $0.2\mu m$ to monitor the distance from the coverslip. The solution temperature was tuned by flowing heat exchanging fluid in an adjacent chamber used in earlier experiments on active engines [1]. Particles were imaged using a Basler Ace 180 kc color camera at $500 frames/sec$. The influence of red laser was eliminated by considering only the green slice of the RGB image and the particle position is tracked to sub-pixel resolution to an accuracy of 5 nm along x-y and 10 nm along z direction using custom built tracking codes in Matlab.

CORRELATIONS AND VORTEXES

In the low Reynolds number regime, as in our experiment, velocity correlations of a colloidal particle in an isolated optical trap are known to decay sharply in timescales of the order of μs. Although motion of the colloidal microsphere through the fluid does generate hydrodynamic flows [2, 3], accounting for the changes in particle motion due to the feedback from these flows is necessary only at sufficiently low viscosity and is negligible in our experiments. Nevertheless, in the presence of another particle in close proximity, hydrodynamic flows could mutually affect each other and with interactions dictated by the Oseen tensor, it can be shown that these could result in an anti-correlated motion [4] along the line joining them. However, as constrained by the fluctuation dissipation relation, these flows do not lead to any net energy transfer, but, the noise correlations do persist longer. We plot the position cross-correlation, $\langle x_1(t)x_2(t+\tau)\rangle$, where x_1, x_2 are the respective displacements of the particles in T1 and T2 along the line joining them, the x-axis for our experiment in Fig. S1(a). As predicted in earlier experiments [4], we observe an initial decrease in $\langle x_1(t)x_2(t+\tau)\rangle$, with maximum anti-correlation at $\approx 6ms$. Also, $\langle x_1(t)x_2(t+\tau)\rangle$ is significantly negative even at large $\tau \approx 25ms$. We exploit this to inject a notable reflux of energy from the ensuing vortexes [5], the active driving in our system to the particle motion. Also, this energy transfer can now be manipulated using solution viscosity as a switch to create reservoirs of high and low energy addition mimicking temperature/activity. In our experiments, we emulated the standard protocol of microengines [1, 6] to operate a Stirling cycle simultaneously on both traps using this inter-trap heat transfer to generate work.

Also, in the main text, we discussed that the position of the particle in the x-y plane decides the amount of light

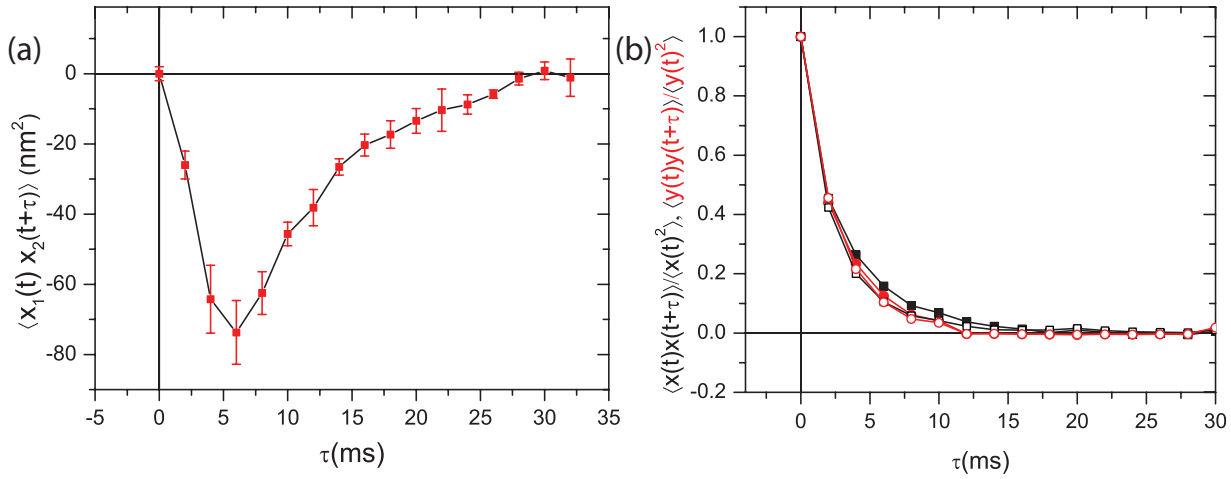

Fig. S 1. Cross-correlation of particle displacements: (a) Cross-correlation, $\langle x_1(t)x_2(t+\tau)\rangle$ between displacements $x1, x2$ of particles trapped in T1 and T2 respectively show strong anticorrelation at $\approx 6ms$. The traps are separated by a distance of $3.6\mu m$ and the solution temperature was maintained at 300K.The correlations, however last up to 25ms. (b) shows auto-correlations along both x and y axes $\frac{\langle x_i(t)x_i(t+\tau)\rangle}{\langle x_i(t)^2\rangle}$ (black square symbols) and $\frac{\langle y_i(t)y_i(t+\tau)\rangle}{\langle y_i(t)^2\rangle}$ (red circular symbols) for particles in the trap L1 (closed symbols) and L2 (open symbols).

scattered, the primary source of non-equilibrium driving in our system. We argued that since the positions in the x-y plane are approximately exponentially correlated, we used a similar profile for noise correlations in calculating thermodynamic quantities. In Fig. S1(b), we plot spatial auto-correlations along both x and y axes for both the trapped particles. Due to the symmetry of the optical trap, its stiffness along x and y axes are almost equal and the position correlations along them are similar. Further, even though the laser intensities $S(L2) = 1.33S(L1)$, difference in their stiffness $\approx 0.8pN/\mu m$ did not produce significantly different correlations. While analytically, the spatial auto-correlations are known to decay as double exponential [7], we observed that this could be approximated for simplifying our calculations to a single exponential with a time constant $\approx 5 - 6ms$. The stochastic thermodynamics model used in our experiments to calculate thermodynamic quantities was based on this assumption. The Brownian dynamics simulations in Fig. 3(f) of the main text used an exponentially correlated noise that decayed over the same order $= 10ms$ of timescales.

An alternative method to model vortexes would be to consider the non-conservative forces as a solenoidal field that generates cross-interactions along the radial, r and vertical directions, z as discussed in previous studies [8] for isolated traps. Key parameters that decide whether such a model can developed are the ratio between the stiffness along the z and r directions, k_z/k_r and the ratio between the non-conservative and conservative forces *eps* as discussed by Pesce. et. al [8] (denoted as ϵ by Pesce. et. al). These can in turn be calculated using r and z autocorrelation functions (ACF) and difference between the cross-correlation functions (DCCF). In Fig. S2 (a) and (b), we plot ACF and DCCF respectively for isolated traps used in our experiments and the corresponding fits to the predicted formulae [8] match the observations of Pesce. et. al [8]. k_z/k_r and ϵ calculated using these fits are presented for the highest input laser intensity S_{max} and bath temperatures T_H (hot) and T_C (cold) in Fig. S2 (c). Also the ratio $k_{1z}/k_{2z} = 1.33$, as in our experiments. We observe that k_z/k_r increases with laser intensity and decreases with temperature. On the other hand, *eps* decreases with S and increases with temperature. As decreasing laser power and increasing temperature have the similar effect of generating free volume for the particle motion, these results concur with the observations of Pesce et.al. Nevertheless, a high value of $eps = 0.11$ implies a significant contribution of the non-conservative forces to particle dynamics, which only increases further due to enhanced hydrodynamics on coupling the particle motions. Developing a solenoidal model to describe coupled engines would not be possible under such conditions.

PROBABILITY CURRENTS AT DIFFERENT EXPERIMENTAL CONDITIONS

In the main text we described that the vortexes are enhanced due to mutual interaction when another particle is introduced in the adjacent trap. Nevertheless, the increase in Q_{Ex} due to this depends on the ambient parameters such as viscosity, separation between the particles etc. as described in Fig.s 1(c) and (d) of the main paper. Here, to reaffirm our results, we demonstrate that the same is also true of the vortexes as well. To this extent, we calculated the probability currents, j due to the

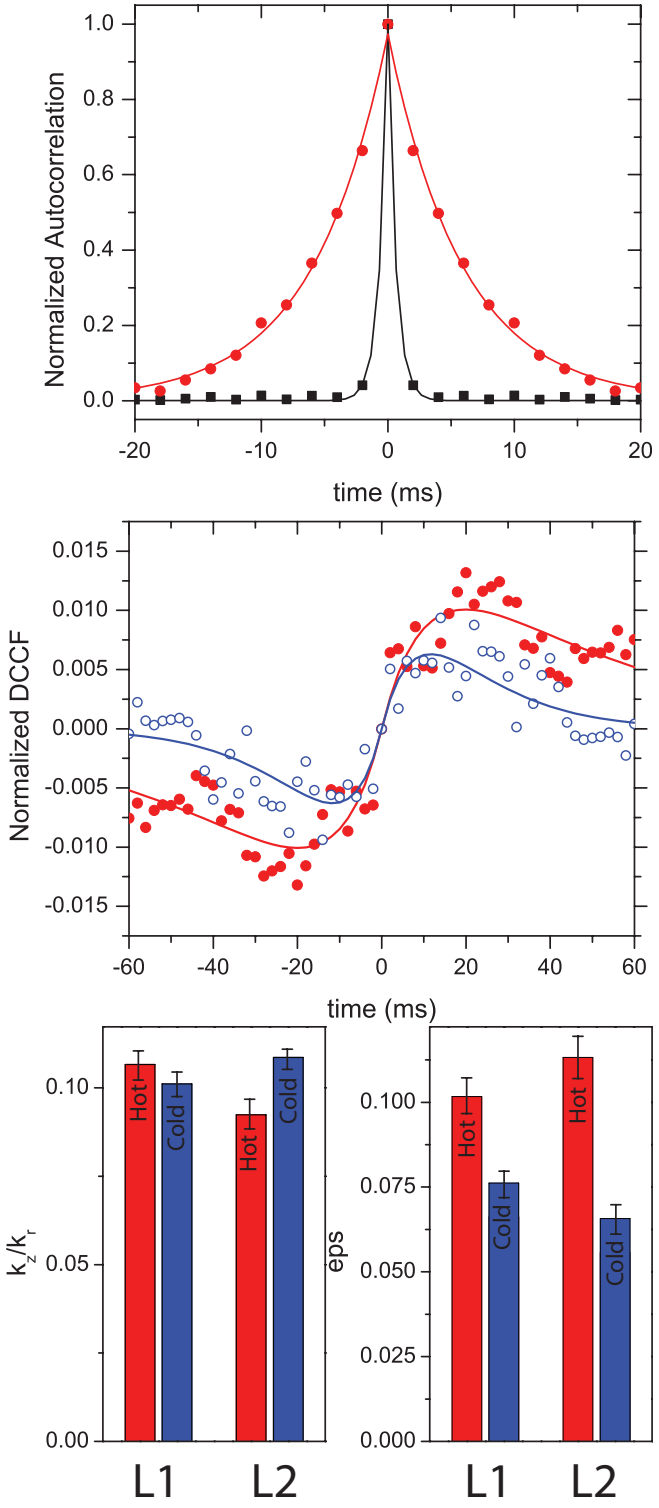

Fig. S 2. **Modeling non-conservative forces as a Solenoidal field. (a)** shows ACF along r (black squares) and z (red circles) co-ordinates for an isolated particle trapped in L2 at a bath temperature T_C at $S = S_{max}$. The solid lines are exponential fits for the ACF. **(b)** shows DCCF for the same particle in a reservoir of temperature T_H (closed red circles) and T_C (open blue circles). The solid lines are fits to the formulae derived by Pesce et.al. The results in **a** and **b** are a reflection of similar observations by Pesce. et al. **c** shows the parameters k_z/k_r and *eps* obtained using the fits in **a** and **b** for the isolated traps L1 and L2 at bath temperatures T_H (hot) and T_C (cold).

interactions - a measure of the disorder in the local flow field at various experimental conditions. The currents are obtained by multiplying the velocity field and the probability distribution represented in Fig. 2. The sum total of magnitude of the probability currents, $\left|j^2\right|$ reflect the disorder in system and entropy production. In Fig. S3, we plot $\left|j^2\right|$ at various experimental conditions. $\left|j^2\right|$ increases with S in the hot reservoir (Fig. S3(a)) and vice versa in the cold reservoir. This matches closely with the observations on Q_{Ex} in Fig. 1(c) reaffirming the hydrodynamic origins of non-conservative interactions. In Fig. S3(b), we plot $\left|j^2\right|$ at various distances of separation. The vortexes decrease with separation of particles in line with our observations in Fig. 1(d) of the main paper. Thus, as anticipated by our observations, the presence of prominent vortexes in isolated traps leads to a greater Q_{Ex}. The change in the vortex pattern in turn is due to the difference in the viscosity of the suspending medium.

PROBABILITY DISTRIBUTIONS ALONG X AND Y-DIRECTIONS

In the main text, we considered the motion only along the z-direction to calculate T_{act}, since the addition of another particle in the adjacent trap causes negligible changes in $P(\Delta x)$ and $P(\Delta y)$ as seen in Fig. 1(b) of the main text. To reaffirm that they are indeed insignificant, we plot $P(\Delta x)$ and $P(\Delta y)$ for T2 before and after introducing the other colloidal microsphere in the neighboring trap in Fig. S4 at the same extreme conditions in Fig. 5 of the main text. From the Fig. S4, the small changes in $P(\Delta x)$ and $P(\Delta y)$ are within the limits of experimental error. Although there is a slight change of statistics in the tails, the combined increase in energy enclosed by $P(\Delta x)$ and $P(\Delta y)$, on coupling, was found to be $\approx 0.05 k_B T_C$. Thus, most of the contributions for an elevated T_{act} arise from the changes in the z-direction.

STOCHASTIC THERMODYNAMICS OF COUPLED ENGINES

To calculate work and efficiency of our engines, we used the framework of stochastic thermodynamics. The equation of motion for an isolated sphere in an optical trap is

$$\gamma(\dot{\mathbf{r}} - v_1'(\mathbf{r}, S)) = -\nabla U_1 + F_{1s}(\mathbf{r}, S) + \xi_1(t) \qquad (1)$$

where, $\gamma = 6\pi\mu(\sigma/2)$ is the friction co-efficient, U is the conservative potential corresponding to the gradient force, F_{1s} is the non-conservative scattering force, ξ_1 is the thermal noise and $v_1'(\mathbf{r}, S)$ is the fluid flow generated by the dissipation of energy input by F_{1s}. In our experiments, we fix the co-ordinate system such that the laser propagates along the z-axis. Apart from displacing the

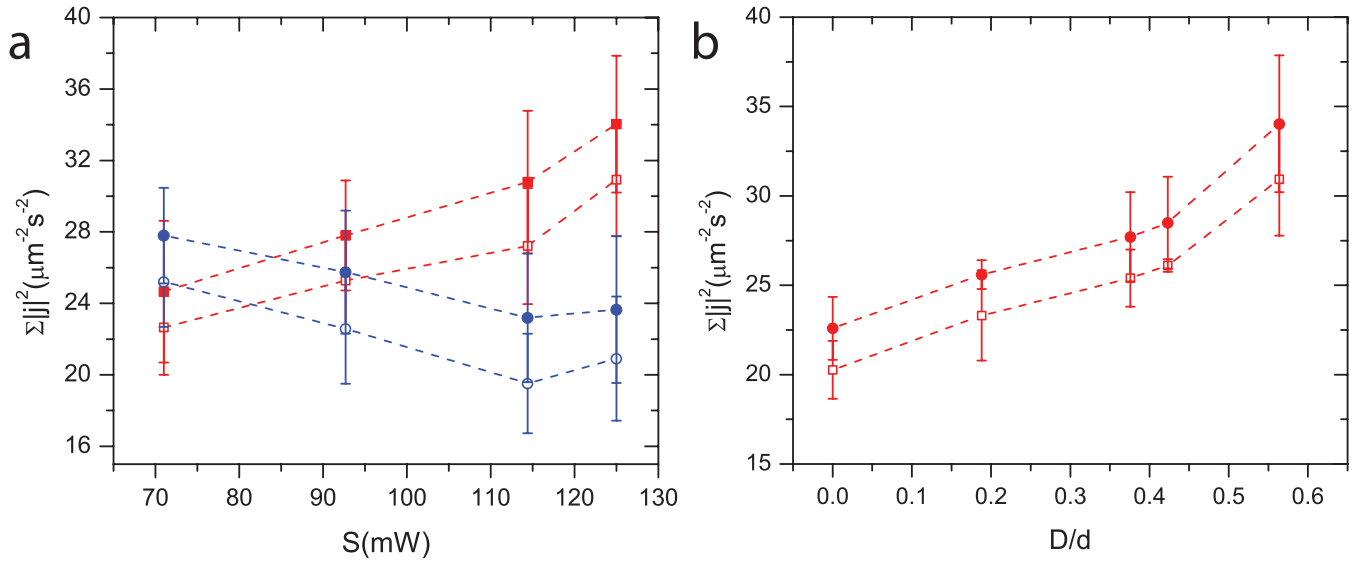

Fig. S 3. Probability currents at different experimental conditions: (a) shows the sum total of magnitude of probability currents $|j^2|$ for particles in both the traps L1 (open symbols) and L2 (closed symbols) when they are in contact with hot (red symbols) and cold (blue symbols) reservoirs at various laser power, S used in the experiment. Probability currents increase with S in the hot reservoir and decrease with S in the cold reservoir in line with our observations in Fig. 1. (b) shows a similar plot of $|j^2|$ for various distances of separation.

mean position away from the origin, as observed in Fig. 3 of the main text, F_{1s} and $v_1'(\mathbf{r}, S)$ are negligible along the x and y axes in comparison with the gradient force. The equation of motion along the z-axis is

$$\gamma \dot{z} = -k_{1z} z + [F_{1s}(\mathbf{r}, S) + \gamma v_1'(\mathbf{r}, S)] + \xi(t) \qquad (2)$$

As noted in the main text, the feedback of energy from the terms in the parenthesis to the particle motion (typically up to 4% of the thermal energy) can be neglected in most experiments [8] and can be treated as perturbations over the equilibrium behavior. Adding another identical particle to an adjacent optical trap induces hydrodynamic interactions between the two particles. The resulting equations of motion along the z-axis would be

$$\begin{aligned}\gamma \dot{z_1} &= -k_{1z} z_1 + c(-k_{2z} z_2 + F_{2s}) + [F_{1s}(\mathbf{r_1}, S_1) + \gamma v_1'] + \xi_1(t) \\ \gamma \dot{z_2} &= -k_{2z} z_2 + c(-k_{1z} z_1 + F_{1s}) + [F_{2s}(\mathbf{r_2}, S_2) + \gamma v_2'] + \xi_2(t)\end{aligned} \qquad (3)$$

where c is the hydrodynamic coupling constant and can be calculated from the Rotne-Prager diffusion tensor to be $c = \frac{3\sigma}{4d} + \frac{\sigma^3}{2d^3}$ (For similar treatments of coupled hydrodynamics see [7, 9, 10]). Proceeding further from this would require an explicit form for F_{is} and v_i'. As discussed in the main text, this can be achieved only in two extremes. While studies in the past have operated in one extreme and tried to arrive at closed form expressions for these by modeling incident laser intensity, apart from addressing general features such as reversal of circulatory flows etc., such approximations have been unable to capture the particle dynamics. In difference with these studies, motivated by the irregular nature of the trajectories that we observed in Fig. 2 of the main text, we modeled the system in the other extreme and approximated these terms to a non-equilibrium noise, $\alpha_i(t) = F_{is} + cF_{js} + \gamma v_i'$ with $i \neq j$. In practice, however, the state of the system lies in between these two extremes, but developing a model in such conditions is inviable using current theoretical frameworks. In this work, we choose to model the system using non-conservative noise. The equations of motion would then be

$$\begin{aligned}\gamma \dot{z_1} &= -k_{1z} z_1 - ck_{2z} z_2 + \alpha_1(t) + \xi_1(t) \\ \gamma \dot{z_2} &= -k_{2z} z_2 - ck_{1z} z_1 + \alpha_2(t) + \xi_2(t)\end{aligned} \qquad (4)$$

Since the observed mean displacement along the z-axis was negligible, we impose $\langle \alpha_i(t) \rangle = 0$. However, since previous studies have noted that the position-auto correlation function along x and y directions decayed as a double exponential [7, 9] (Plotted in Fig. S1(b) for our data), and the scattering force crucially depends on the particle position, as a first order approximation, we choose $\langle \alpha_i(t) \alpha_i(t') \rangle = A_i e^{-\frac{t-t'}{t_\alpha}}$. Analogous to the case of the isolated trapped particle, we define the heat transferred to the particle i, Q_i in a time interval τ as

$$Q_i = -\int_0^\tau (-\gamma \dot{z_i} + \alpha_i(t) + \xi_i(t)) \dot{z_i} dt \qquad (5)$$

Such a definition treats α_i as a driving active noise analogous to an active Brownian particle and any energy received from F_{is} and $v_i'(\mathbf{r}, S)$ is similar to that received from the thermal reservoir except through different statistics. Intuitively, this term corresponds to the

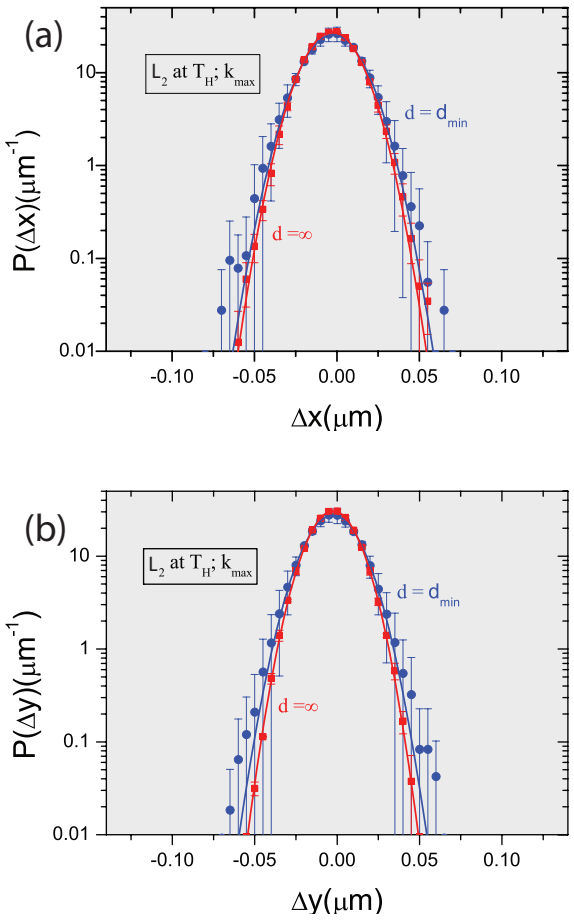

Fig. S 4. Probability distributions along x and y directions: (a) and (b) show $P(\Delta x)$ and $P(\Delta y)$ respectively for a particle in T2 before(red squares) and after(blue circles) introducing an identical particle in T1 at the same extreme conditions in Fig. 5 of the main text. The solid lines represent Gaussian fits for the same.

heat rejected to the surroundings in the case of an isolated optical trap that is now being reused by the particle in the adjacent trap. Such a possibility arises only because this heat was reused before the hydrodynamics in the medium dissipated it into the surroundings. Using Eqn. (4), we can rewrite this as

$$Q_i = -\int_0^\tau (k_{iz} z_i + c k_{jz} z_j)\dot{z}_i dt; i \neq j \tag{6}$$

Following Berut et.al. [7] we decompose this into two terms for each particle as

$$\begin{aligned} Q_{ii} &= -\int_0^\tau k_{iz} z_i \dot{z}_i dt \\ Q_{ij} &= -\int_0^\tau c k_{jz} z_j \dot{z}_i dt; i \neq j \end{aligned} \tag{7}$$

While the first term can be represented as a conservative force and simplifies to $Q_{ii} = -k_{iz}\left[\frac{1}{2}z_i^2\right]_0^\tau$, the second term represents the heat transferred between the two particles.

Performing work on the system of coupled particles requires varying either the conservative potential, $U_i = \frac{1}{2}k_{iz}z_i^2$ or the hydrodynamic coupling, $f_j = c k_{jz} z_j$ between them. Since c is maintained constant during the engine protocols used in our experiment, both processes occur simultaneously. To calculate the work done during an isothermal process where the parameters k_{1z} and k_{2z} are linearly increased/decreased, we used the standard definitions of Stochastic thermodynamics. Work done, W_i can be decomposed into two terms as

$$\begin{aligned} W_i &= W_{ii} + W_{ij}; i \neq j \\ W_{ii} &= \int_0^\tau \frac{\partial U_i}{\partial t} dt = \int_0^\tau \frac{1}{2}\dot{k_{iz}} z_i^2 dt \\ W_{ij} &= \int_0^\tau f_j \circ \dot{z}_i dt = \int_0^\tau c k_{jz} z_j \dot{z}_i dt; i \neq j \end{aligned} \tag{8}$$

where, W_{ii}s are work done by conservative optical forces and W_{ij}s are those by non-conservative hydrodynamic coupling. The total efficiency of the engine can be defined as

$$\mathcal{E}_i = \frac{\langle W_i \rangle}{\langle Q_i \rangle} \tag{9}$$

where, W_i is the average work done at the end of each cycle and Q_i is the heat transferred to the engine from the hot reservoir.

Averaging considerations in calculating thermodynamic quantities

While Eq.s (8) provide a recipe to calculate the work done, the integrals should converge over a reasonable experimental duration to achieve appropriate averaging. To determine the averaging required for convergence of W_{ii}s and W_{ij}s, we observe their probability distributions along the hot isotherms calculated over a single time step of our observations = 2ms in Fig. S5. The trajectory of the particle during the isotherm was divided into 10 equal bins such that change in k_{iz} was negligible across each of them. W_{ii} and W_{ij} were calculated using Eq.s (8) over each time step of measurement and probability distributions, $P(W_{ii})$ and $P(W_{ij})$ corresponding to each bin were plotted independently. Fig.s S5(a) and (b) show such distributions of W_{ii}s, where $k1 \rightarrow k10$ represent $P(W_{ii})$ plotted for bins with a decreasing order in k_{iz} from k_{max} to k_{min}. $W_{ii} < 0$ as $z_i^2 > 0$ and $\dot{k_{iz}} < 0$ during isothermal expansion and indicates work done by the system on the surroundings. The summation of these W_{ii}s over the isotherm sampled $n = 3500$ times in our experiments converges as in the case of isolated engines to $n\langle W_{ii}\rangle < 0$ [6]. Similar distributions for W_{ij}s (Fig. S5 (c) and (d)), however, are distributed equally about

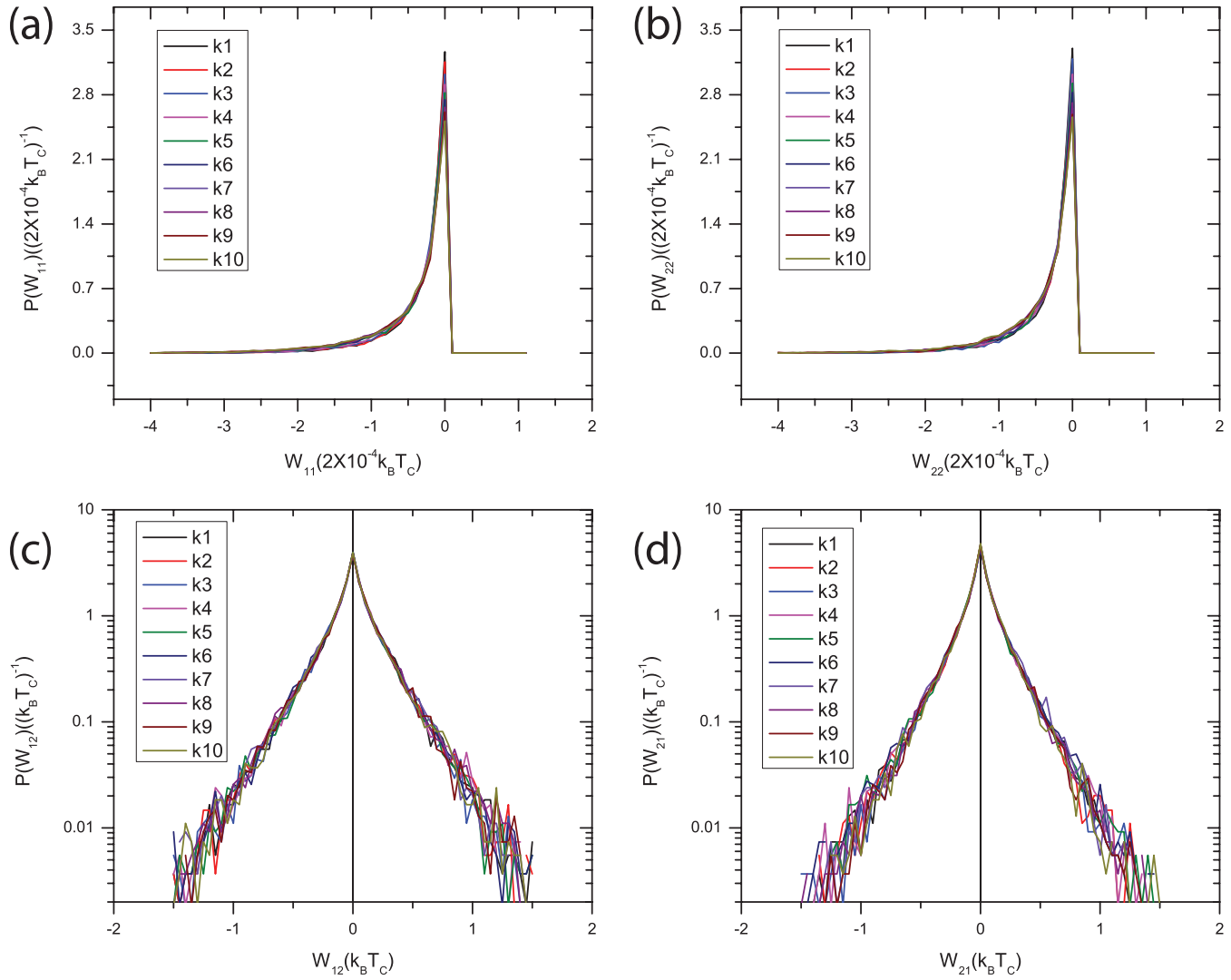

Fig. S 5. Work distributions along the hot isotherm: (a) - (d) shows probability distributions of work done by the engine W_{11}, W_{22}, W_{12} and W_{21} respectively for various k_{iz} along the hot isotherm. $k1 \rightarrow k10$ represent $P(W_{ii})$ and $P(W_{ij})$ plotted for bins with a decreasing order in k_{iz} from k_{max} to k_{min}.

$W_{ij} = 0$ with a standard deviation of $\sigma(W_{ij}) = 0.5 k_B T_C$. By central limit theorem, the probability distribution of the summation over n terms along the isotherm would have a standard deviation $0.5\sqrt{n} k_B T_C$ and a mean 0. Thus, $\langle W_{ij} \rangle = 0$ if the isotherm is executed a sufficiently large number of times and averaged. Over finite experimental durations, however, the error in measuring $\langle W_{ij} \rangle$ could be significant. Reducing the error in such a measurement, the standard error of mean to even 10% of $\sigma(W_{ij})$ requires us to average over $100Xn = 350,000$ cycles. Such large number of cycles are impractical in our experiments. In our analysis, we assumed $\langle W_{ij} \rangle = 0$, the average expected from central limit theorem.

Active temperature

Given $\langle W_{ij} \rangle = 0$, we could define an active temperature as in previous studies. The total work done over the Stirling cycle, W can be written as summations over the hot and cold isotherms that are performed at the same rate in our experiment i.e. $\dot{k_z}(hot) = -\dot{k_z}(cold)$

$$\begin{aligned} W &= \sum_{hot} W_{ii} + \sum_{cold} W_{ii} \\ &= \frac{1}{2\nu} \dot{k}(hot) \left[\sum_{hot} z_i^2 - \sum_{cold} z_i^2 \right] \end{aligned} \tag{10}$$

where ν is the sampling frequency = 500Hz in our experiment. Using equipartition theorem, we could define active temperature as $T_{iact} = \frac{k_z \langle z_i^2 \rangle}{k_B}$. Average work done

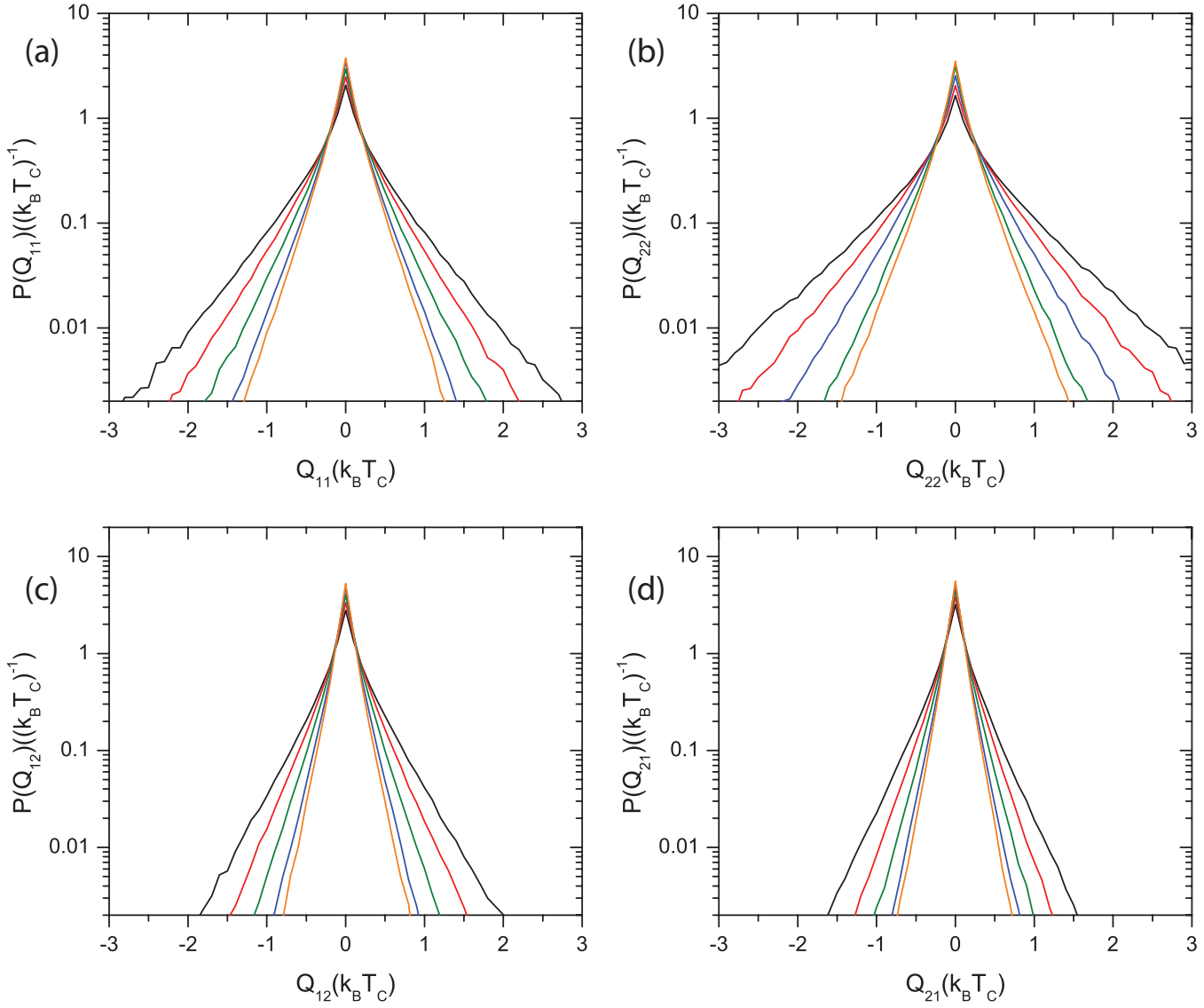

Fig. S 6. Simulated heat flows at various $|\alpha_{\mathbf{i}}|$ at constant **c**: (a) - (d) shows probability distributions of heat fluxes Q_{11}, Q_{22}, Q_{12} and Q_{21} respectively for the noise intensities $|\alpha_1|/\sqrt{2\gamma k_B T_C} = 1$ (orange), 5 (blue), 10 (green), 15 (red) and 20 (black) at constant $c = 0.5$.

over the Stirling cycle can then be written as

$$\langle W \rangle = \frac{1}{2\nu k_B} \dot{k}(hot) \left[\sum_{hot} \frac{T_{iact}(hot) - T_{iact}(cold)}{k_{iz}} \right] \quad (11)$$

Thus, average work done over the cycle would be proportional to the difference in T_{act} between the hot and cold isotherms. In our experiments in Fig. 5 of the main text, we observed that this difference increases due to the mutual interactions and leads to better performance.

Finally, since we did not observe any changes in the probability distributions along x and y axes as discussed in Fig. S4, the above analysis can be used to calculate performance along these directions assuming $\alpha_i = 0$.

BROWNIAN DYNAMICS SIMULATIONS

In our analysis in Fig. 3(f) of the main text, we simulated the equations of motion Eq. (4) through Brownian dynamics algorithms. Particle trajectories were computer generated using conventional Brownian dynamics algorithm [11, 12] for a time step $dt = 0.2ms$. We observed that dt was sufficiently small that more sophisticated algorithms such as stochastic Runge-Kutta algorithm, stochastic expansion etc. [11, 12] resulted in changes only in the fourth significant figure.

In our discussions in the main text, we noted that unlike experiments, the simulations allowed us to independently vary $|\alpha_i|$ and c and this can be leveraged to obtain insights into the nature of the interactions. To this ex-

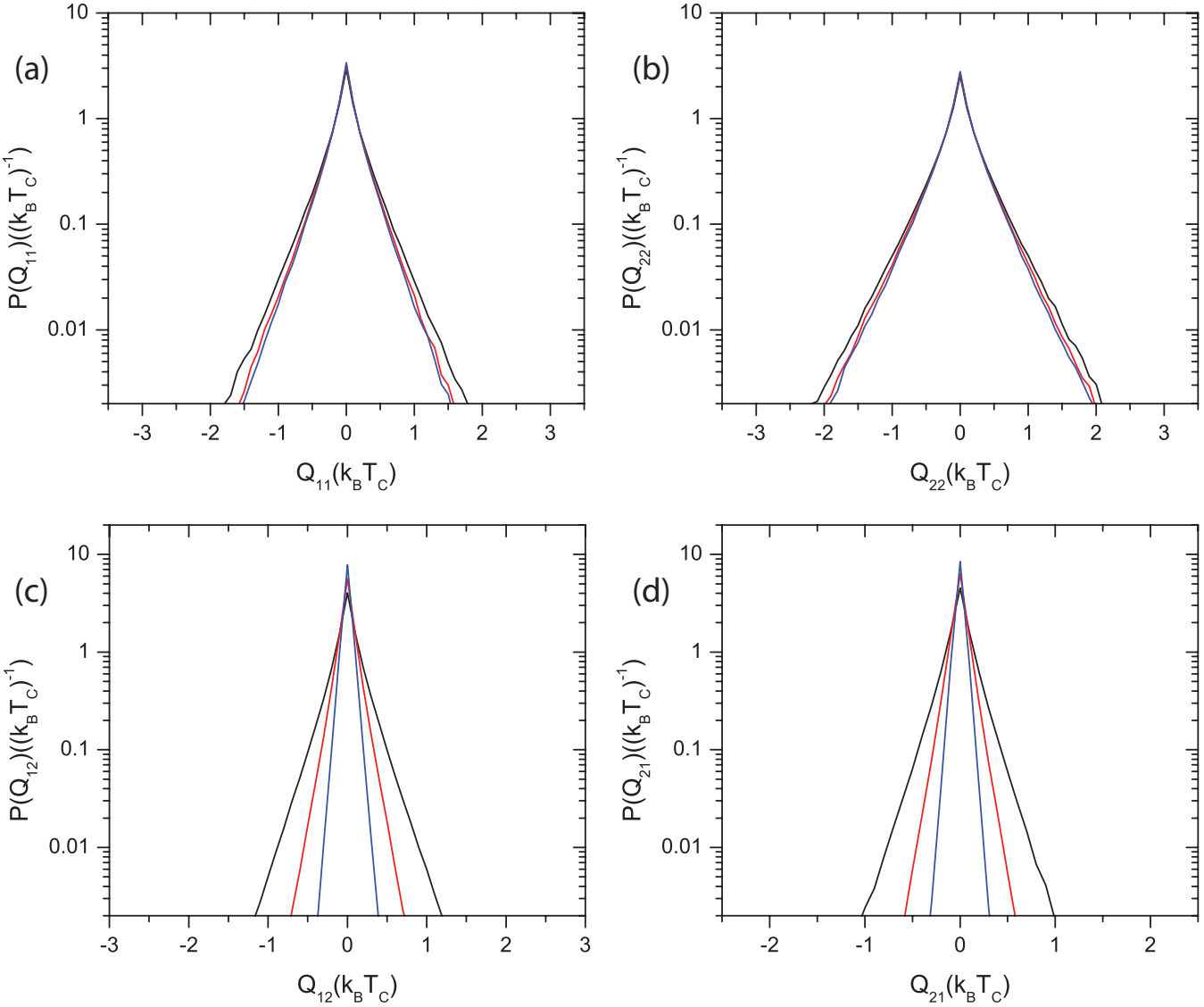

Fig. S 7. Simulated heat flows at various **c** at constant $|\alpha_\mathbf{i}|$: (a) - (d) shows probability distributions of heat fluxes Q_{11}, Q_{22}, Q_{12} and Q_{21} respectively for various $c = 0.5$ (black), 0.3 (red) and 0.15 (blue) for noise intensity $|\alpha_1|/\sqrt{2\gamma k_B T_C} = 10$.

tent, we varied the magnitude of the noise, $|\alpha_i|$ while c was maintained constant and observed the corresponding variations in heat currents in Fig. S6. The results in Fig. S6 closely match the experimental counterparts in Fig.s 3(a)-(d) of the main text. Similar observations made by alternately fixing $|\alpha_i|$ as c was varied are presented in Fig. S7. In contrast to Fig. S6, we observe that the changes in stochastic heat currents in Fig. S7 are relatively small. However, the experimental data in which these two cannot be independently varied did show a significant increase in standard deviations in heat transfer (Fig. 3(a)-(d)). Thus, while arranging the optical traps at close separation does increase the hydrodynamic coupling between them, the increase in mutual interactions arise largely from the associated increase in Brownian vortexes.

Finally, in Fig. S8 we explore the changes in heat flow as we vary the simulation parameters. All deterministic parameters were maintained at their approximate experimental values i.e. $k_{1z} = 0.49pN/\mu m$, $k_{2z} = 0.66pN/\mu m$, $T = 300K$, $dt = 0.2ms$, $\mu = 0.8mPa.s$, $\sigma = 2\mu m$, $\langle|\alpha_2|\rangle/\langle|\alpha_1|\rangle = 1.33$. To quantify the interactions, we used the active temperature T_{iact} defined in the previous section. T_{iact} was observed to increase with $|\alpha_1|$ for both $c = 0.5$ and 0.15 (Fig. S8), but it was significantly higher at close separation ($c = 0.5$). In our experiments, the strength of interactions $|\alpha_i|$ changes with k_{1z} and k_{2z} during the isotherms, this could lead to different T_{act} along them as observed in Fig. 5 of the main paper. Further, varying $\langle|\alpha_2|\rangle/\langle|\alpha_1|\rangle$ which we had fixed at 1.33 could also allow us to adjust the model to fit the experimental data. In Fig. S8(b), we show that by changing it

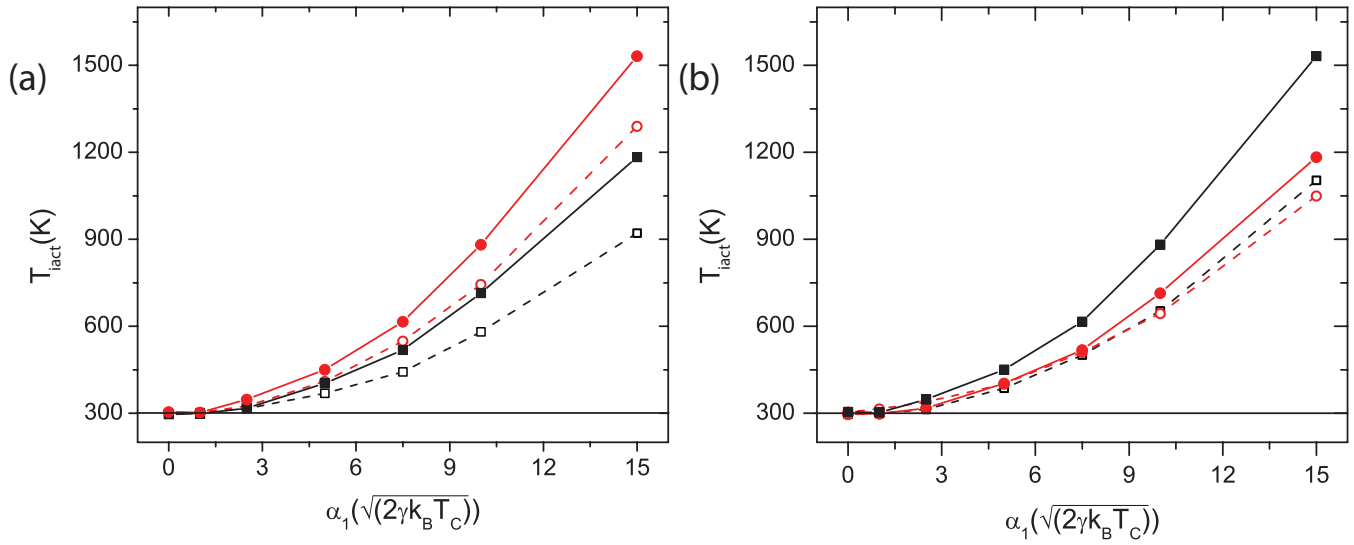

Fig. S 8. Adjusting T_{iact} with simulation parameters: (a) shows variations in T_{1act} (red circles) and T_{2act} (black squares) with $|\alpha_1|$ for $c = 0.5$ (closed symbols) and 0.15 (open symbols). (b) shows a similar plot for various ratios of noise intensities $\langle|\alpha_2|\rangle/\langle|\alpha_1|\rangle = 1.33$ (closed symbols) and 1 (open symbols).

to 1, we could even reach a scenario where $T_{1act} = T_{2act}$. In conclusion, while the heat flows arising from interactions due to non-conservative flows can be captured by our model, it does not predict relations between T_{iact} and k_{iz}. Arriving at such relations continues to remain an open question after our simulations. Nevertheless, the model can be appropriately adjusted with parameters $|\alpha_1|$ and $\langle|\alpha_2|\rangle/\langle|\alpha_1|\rangle$ to capture the heat flows and understand the increase in performance.

It is to be noted that the assumption that non-conservative forces are entirely chaotic might still be an overstatement and might lead to greater dissipation. While this might overestimate the magnitude of the non-conservative forcing, the heat flows calculated from them were similar to experimental observations in Fig. 3 of the main paper and justifies our assumptions. Further, tuning the parameter space in the model allows us to obtain a qualitative understanding of the results observed in the main paper.

MOVIE CAPTION

Movie S1. Microscope video of the realization of coupled heat engine for the closest separation d = 3.6 μm : Colloidal micospheres of diameter 2.03 μm are trapped in focused laser beams L1 and L2. The temperature of the suspending medium, marked at the top left corner, is varied by passing a heat exchanging fluid in an adjacent channel. The isochoric processes are marked by the shining of the red laser

[1] Sudeesh Krishnamurthy, Subho Ghosh, Dipankar Chatterji, Rajesh Ganapathy, and AK Sood, "A micrometre-sized heat engine operating between bacterial reservoirs," Nature Physics **12**, 1134–1138 (2016).

[2] John C Crocker, "Measurement of the hydrodynamic corrections to the brownian motion of two colloidal spheres," The Journal of chemical physics **106**, 2837–2840 (1997).

[3] Giuseppe Pesce, Giorgio Volpe, Giovanni Volpe, and Antonio Sasso, "Long-term influence of fluid inertia on the diffusion of a brownian particle," Physical Review E **90**, 042309 (2014).

[4] Jens-Christian Meiners and Stephen R Quake, "Direct measurement of hydrodynamic cross correlations between two particles in an external potential," Physical review letters **82**, 2211 (1999).

[5] Michel de Messieres, Natalia A Denesyuk, and Arthur La Porta, "Noise associated with nonconservative forces in optical traps," Physical Review E **84**, 031108 (2011).

[6] Valentin Blickle and Clemens Bechinger, "Realization of a micrometre-sized stochastic heat engine," Nature Physics **8**, 143–146 (2012).

[7] Antoine Bérut, Alberto Imparato, Artem Petrosyan, and Sergio Ciliberto, "Stationary and transient fluctuation theorems for effective heat fluxes between hydrodynamically coupled particles in optical traps," Physical review letters **116**, 068301 (2016).

[8] Giuseppe Pesce, Giorgio Volpe, Anna Chiara De Luca, Giulia Rusciano, and Giovanni Volpe, "Quantitative assessment of non-conservative radiation forces in an optical trap," EPL (Europhysics Letters) **86**, 38002 (2009).

[9] Antoine Bérut, Alberto Imparato, Artyom Petrosyan, and Sergio Ciliberto, "Theoretical description of effective heat transfer between two viscously coupled beads," Physical Review E **94**, 052148 (2016).

[10] Salvador Herrera-Velarde, Edith C Euán-Díaz, Fidel Córdoba-Valdés, and Ramón Castaneda-Priego, "Hydrodynamic correlations in three-particle colloidal systems in harmonic traps," Journal of Physics: Condensed Matter **25**, 325102 (2013).

[11] AC Brańka and DM Heyes, "Algorithms for brownian dynamics simulation," Physical Review E **58**, 2611 (1998).

[12] AC Brańka and David M Heyes, "Algorithms for brownian dynamics computer simulations: Multivariable case," Physical Review E **60**, 2381 (1999).